Suns-ILIT: Contact-less determination of local solar cell current-voltage characteristics

Wolfram Kwapil[a,b,*], Sven Wasmer[a], Andreas Fell[a], Johannes M. Greulich[a], Martin C. Schubert[a]

[a] Fraunhofer Institute for Solar Energy (ISE), Heidenhofstr. 2, 79110 Freiburg, Germany
[b] University Freiburg, Department of Sustainable Systems Engineering (INATECH), Emmy-Noether-Str. 2, 79110 Freiburg, Germany

ARTICLE INFO

ABSTRACT

We present a novel method to analyze the local current-voltage I-V characteristics of both solar cells and cell precursors. The method, which we call "Suns-ILIT", is based on illuminated lock-in thermography (ILIT) measurements and photoluminescence imaging (PLI) in open-circuit conditions with varying illumination intensities. Compared to conventional techniques for the determination of local solar cell parameters, the advantage of Suns-ILIT lies in the high accuracy while imposing minimal requirements on the sample. In particular, no electrical contact to the sample is needed. We derive the necessary equations from the contributions to the power dissipation and investigate the impact of the Peltier heating and cooling on the final outcome. The method is applied to a standard multicrystalline silicon PERC solar cell for demonstration.

1. Introduction

Since its first introduction by Sinton and Cuevas in 2000, Suns-V_{OC} measurements have found widespread use for the characterization of solar cells [1]. This is due to a number of differences between Suns-V_{OC} measurements and related methods such as J_{SC}-V_{OC}, dark or illuminated I-V characterization, some of which are advantageous. Instead of measuring the extracted current at varying working points of the test sample, the Suns-V_{OC} technique is based on the conversion of the illumination intensity, as determined by a calibrated reference solar cell, into a measure of recombination current (e.g. by using the calculated photogeneration of the sample equal to the recombination current under open-circuit conditions or its short-circuit current). Hence, the resulting I-V curve is only little influenced by the series resistance affecting the current extraction. As a consequence, on the one hand solar cell properties governed by processing steps other than the metallization can be investigated. On the other hand, the requirements on both the sample properties and the probe station are lowered. In principle, samples even in very early processing stages just after junction formation can be inspected, using a simple and rough two point probe to determine the voltage.

By fitting the two-diode model [2] to the I-V data, the solar cell parameters retrieved from Suns-V_{OC} measurements are similar to series resistance-corrected dark I-V results: the saturation current densities j_{01} and j_{02} from the first and the second diode, respectively, the ideality factor n_2 of the second diode (if allowed to float) and the shunt resistance R_p.

For an analysis of the spatial distribution of solar cell parameters, several methods have been proposed. For example, the relation between the photoluminescence intensity (PLI) and the implied (local) V_{OC} was exploited for global [3] or spatially resolved [4,5] extraction of solar cell parameters analogous to Suns-V_{OC} measurements. One major drawback of this "Suns-PLI" approach is that no information about the local recombination *current* distribution is available. Hence, an average value equal to the homogeneous photocurrent is assumed, with drawbacks similar to those discussed in the previous paragraph. Further approaches based on a series of electro- and/or photoluminescence images have been developed that require electrically contacting the solar cell and performing four-wire measurements of current and voltage [6–9]. Another method based on lock-in thermography measurements in the dark (DLIT) called "local I-V" was proposed by Breitenstein in 2011 [10,11]. In this method, the measured power dissipation is transformed into measures of the local current density and voltage. Whereas "local I-V" thus corresponds to dark I-V measurements, we want to demonstrate a local solar cell parameter characterization method equivalent to Suns-V_{OC} curves using illuminated lock-in thermography (ILIT) [12], which we will call "Suns-ILIT" in the following. Expanding the previous Suns-PLI method with measurements of the current distribution, it features all the advantages coming with the technique. Suns-ILIT does not need any probing of the sample, thus

---

imposing few restrictions on sample properties. In addition, the variation of the illumination wavelength and hence the absorption depth offers the possibility to differentiate the influence of front, bulk and rear properties on the solar cell performance or to distinguish between different layers in tandem cell devices.

The present contribution focuses on the theoretical background and the approach of the novel method, including an exemplary measurement on a standard solar cell. A detailed study of cell precursors and solar cells using Suns-ILIT and a comparison of the results with measurements of conventional techniques will be presented in a separate upcoming publication.

2. Theory

Lock-in thermography is a camera-based method to image the spatial distribution of the temperature modulation due to periodic excitation in a test sample. In the case of DLIT, the calibration for power dissipation is then (in most cases) straightforward: the product of current and voltage introduced into the solar cell must equal the DLIT signal sum. Since the illumination during ILIT measurements adds a second excitation source, the calibration for power is slightly more complex. A convenient way is to measure the sample at two different working points, e.g. under j_{SC}- and maximum power point (MPP) conditions, keeping the illumination intensity constant [12]. The difference between both signal sums must equal the difference in the extracted power.

However, this calibration method requires finished solar cells and satisfactory series resistance values allowing for significant current extraction. If unfinished solar cells or imperfectly metallized samples are to be investigated, a robust way is to calibrate for the total absorbed power P_{in} [12]:

$$(1 - r(\lambda))E_{ph}(\lambda)\Phi_{in}(\lambda)A = P_{in} \tag{1}$$

with $r(\lambda)$ the share of the photon flux at wavelength λ of the incident light that is not absorbed by the solar cell (reflection and transmission, including reflection and absorption at the front metallization), $E_{ph}(\lambda)$ the photon energy, $\Phi_{in}(\lambda)$ the photon flux, and A the solar cell area. The photon flux can be determined using a calibrated reference solar cell. Neglecting transmission, the reflectivity of the sample at the specified wavelength needs to be known.

In order to evaluate j-V curves, the power density images have to be transformed into maps of the current density and voltage distributions. Again, this step is straightforward in most cases of DLIT measurements, at least as long as vertical current flows are dominant (front/rear contact design). Then, the power dissipation is only composed of the electrical power contribution and Joule heating, which can easily be converted into recombination current. A thorough description can be found in Ref. [13].

In contrast, the difficulty of Suns-ILIT lies in the exact differentiation between the various contributions to the power signal. This is mainly due to two reasons: (i) Illumination causes a significant background signal which needs to be carefully taken into account. (ii) Suns-ILIT is based on measurements under V_{OC}-conditions. Since no current is extracted, all absorbed power needs to be dissipated inside the solar cell. Inhomogeneities of the recombination properties in the solar cell lead to significant *lateral* current flows, invalidating simplifications inherent to strictly vertical current flows [14].

2.1. Determination of the recombination current

At the end of this paragraph, we will arrive at two relatively simple, intuitive equations for the determination of the recombination current distribution j_{rec} from V_{OC}-ILIT images calibrated to power densities. However, due to the abovementioned difficulties coming with lateral balancing currents, it is instructive to derive the relevant equations from the different contributions to the power dissipation [13,14]. Thus,
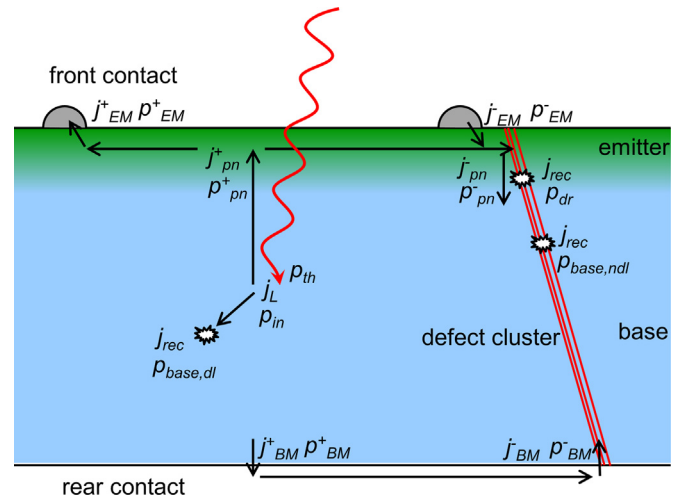

Fig. 1. Sketch of the current flows in a solar cell under V_{OC}-conditions and the abbreviations used in the text.

the underlying assumptions can be critically assessed and the validity for different sample architectures can be checked. Note that a similar treatment of determining recombination currents from V_{OC}-ILIT images in particular can also be found in [15].

In Fig. 1, a simple sketch of possible current paths in a solar cell under open-circuit conditions with corresponding power density contributions is shown. As soon as minority carriers reach the pn-junction and become majority carriers, the carriers are free to move towards highly recombination-active regions such as grain boundaries or dislocation clusters. Hence, the simplified one-dimensional band diagram shown in Fig. 2 is only intended to visualize the different physical processes leading to power dissipation. They are explained in detail in the following. Please note that for better readability, the indices xy, indicating that the power density contributions and current densities p and j, respectively, as well as in the local open-circuit voltage V_{OC} are *local* properties, are omitted in the following equations.

In principle, the number of electron-hole pairs and hence the total recombination current density generated by the incident photo current j_L can be easily calculated assuming one pair per photon:

$$p_{in} = j_L \frac{E_{ph}}{q}. \tag{2}$$

Here, q signifies the elementary charge and p_{in} is the absorbed power density. If the illumination is homogeneous, j_L is distributed
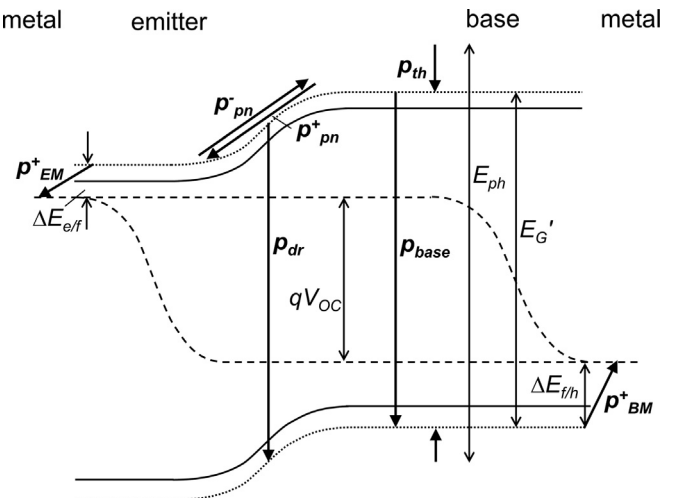

Fig. 2. Sketch of the power dissipation contributions and the related energies.

homogeneously apart from shading by the front metallization. As mentioned above, the currents redistribute, hence the measured signal differs from (2).

In the location of the electron-hole pair generation, the charge carriers thermalize quickly, contributing an amount of

$$p_{th} = j_L \left(\frac{E_{ph}}{q} - \frac{E_G{'}}{q} \right) \tag{3}$$

to the total signal. The value $E_G{'}$ denotes the difference between the mean energies of electrons in the conduction band and holes in the valence band and is generally larger than the band gap energy E_G. The thermalization is laterally homogeneous if the illumination is homogeneous.

If charge carriers recombine within one diffusion length before being separated by the pn-junction, they release

$$p_{base,dl} = j_{base,dl} \left(\frac{E_G{'}}{q} \right), \tag{4}$$

with $j_{base,dl}$ being the diffusion-limited recombination current density in the bulk. It depends on the carrier lifetime distribution involving both material and surface effects and is therefore laterally inhomogeneous in many cases.

When the charge carriers reach the pn-junction, they accelerate in the electric field, transforming their kinetic energy into heat via interactions with the lattice. The amount of power delivered in that process equals

$$p_{pn}^+ = j_{pn}^+ \left(\frac{E_G{'}}{q} - V_{OC} - \frac{\Delta E_{e/f}}{q} - \frac{\Delta E_{f/h}}{q} \right), \tag{5}$$

where j_{pn}^+ signifies the current density crossing the pn-junction and $\Delta E_{e/f}$ and $\Delta E_{f/h}$ are the differences between the mean electron energy and electron quasi-fermi energy level and between the hole quasi-fermi energy level and the mean hole energy, respectively. The meaning of these values is discussed further below.

Once the carriers are free to move as majorities, they may recombine anywhere in the solar cell depending on local recombination rates and on the series resistance between the location where the carriers have crossed the pn-junction and the recombination-active regions. A critical issue in the present consideration is the path the carriers take until they recombine. If the path of least resistance involves transport through the metallization, the power contributions

$$p_{EM}^+ = j_{EM}^+ \frac{\Delta E_{e/f}}{q} \text{ and } p_{BM}^+ = j_{BM}^+ \frac{\Delta E_{f/h}}{q} \tag{6}$$

are generated in the locations where the electrons and the holes cross into the metallization, respectively (Peltier heat generated). The abbreviations *EM* and *BM* stand for emitter-metallization and base-metallization, respectively. Since no current is extracted, all carriers have to cross again from the metallization into the emitter / base before recombining,

$$p_{EM}^- = -j_{EM}^- \frac{\Delta E_{e/f}}{q} \text{ and } p_{BM}^- = -j_{BM}^- \frac{\Delta E_{f/h}}{q}, \tag{7}$$

which is the reverse process of (6) (Peltier cooling).

Before they recombine, the carriers have to gain energy in order to cross the barrier

$$p_{pn}^- = -j_{pn}^- \left(\frac{E_G{'}}{q} - V_{OC} - \frac{\Delta E_{e/f}}{q} - \frac{\Delta E_{f/h}}{q} \right), \tag{8}$$

being the reverse process of (5). It is irrelevant whether the recombination happens in the depletion region or in the base. Whereas in the former case, two particles share the necessary energy, in the latter case, only one carrier is involved.

When recombining, a power of

$$p_{dr} = j_{dr} \left(\frac{E_G{'}}{q} \right) \tag{9}$$

and

$$p_{base,ndl} = j_{base,ndl} \left(\frac{E_G{'}}{q} \right) \tag{10}$$

is released in the depletion region ('*dr*') or the base, respectively. The abbreviation '*ndl*' stands for 'not diffusion-limited'.

The recombination power density p_{rec} is then

$$p_{rec} = p_{base,dl} + p_{dr} + p_{base,ndl}, \tag{11}$$

each process being associated with the same energy release of $E_G{'}/q$.

The local power signal p consists of the sum of all above mentioned processes:

$$p = p_{th} + p_{pn}^+ + p_{EM}^+ + p_{BM}^+ + p_{EM}^- + p_{BM}^- + p_{pn}^- + p_{rec}. \tag{12}$$

In inhomogeneous devices, j_{rec} is not equal to j_L (only $I_{rec} = I_L$). In order to find j_{rec}, we make use of the conservation law that all the generated current j_L must go somewhere. We can discriminate two cases:

2.1.1. Un-metallized samples

For illustration purposes, let us first consider an area of high carrier lifetime / low recombination rate in an un-metallized sample: After initial thermalization, minority carriers not recombining within one diffusion length cross the pn-junction (termed j_{pn}^+). After that, some carriers are immediately re-injected in the same location and recombine either in the depletion region or in the base while others move laterally, mostly towards highly recombination-active regions. Due to this movement, in a high-lifetime area the current j_{pn}^+ is larger than the re-injected current j_{pn}^-. For the calculation of Eq. (12), the re-injected carriers can be treated as if these carriers never crossed the pn-junction because their contributions to p_{pn}^+ and p_{pn}^- cancel. Hence, the local power signal only contains the Peltier heating of the carriers that cross the pn-junction *and* eventually flow away.

One of the central equations (the conservation law) for un-metallized samples is therefore:

$$j_L = j_{pn,net} + j_{rec}, \tag{13}$$

where $j_{pn,net}$ denotes the local net pn-junction current,

$$j_{pn,net} = j_{pn}^+ - j_{pn}^-. \tag{14}$$

In highly recombination-active regions, all locally generated carriers recombine and additional carriers arrive from the high lifetime regions, which means that the local $j_{pn,net}$ is negative.

From Eq. (12), the measured total power dissipation in an un-metallized sample is

$$p = j_L \bullet \left(\frac{E_{ph}}{q} - \frac{E_G{'}}{q} \right) + j_{pn,net} \bullet \left(\frac{E_G{'}}{q} - V_{OC} - \frac{\Delta E_{e/f}}{q} - \frac{\Delta E_{f/h}}{q} \right)$$
$$+ j_{rec} \bullet \frac{E_G{'}}{q}. \tag{15}$$

Together with Eq. (13), we find

$$j_{pn,net} = \frac{p_{in} - p}{V_{OC} + \frac{\Delta E_{e/f}}{q} + \frac{\Delta E_{f/h}}{q}} \tag{16}$$

and the calculation of j_{rec} is straightforward once the denominator of Eq. (16) is known, see further below.

2.1.2. Metallized samples

The case of metallized solar cells is more complex since the metallization offers additional paths for lateral balancing currents. With the same reasoning as above, Eq. (13) has to be extended, reading

$$j_L = j_{pn,net} + j_{EM,net} + j_{BM,net} + j_{rec,} \tag{17}$$

where we define local net "Peltier" currents $j_{EM,net}$ and $j_{BM,net}$ in analogy to Eq. (14), for example

$$j_{EM,net} = j_{EM}^+ - j_{EM}^-. \tag{18}$$

Of course, the "Peltier" currents are non-zero only in regions where there is an electrical contact between silicon and metallization. And even then, the range of possible values for $j_{EM,net}$ and $j_{BM,net}$ is

$$0 \le j_{EM,net}, j_{BM,net} \le j_{pn,net}. \tag{19}$$

Finally, the total power dissipation is:

$$p = j_L \cdot \left(\frac{E_{ph}}{q} - \frac{E_G'}{q} \right) + j_{pn,net} \cdot \left(\frac{E_G'}{q} - V_{OC} - \frac{\Delta E_{e/f}}{q} - \frac{\Delta E_{f/h}}{q} \right)$$
$$+ j_{EM,net} \cdot \left(\frac{\Delta E_{e/f}}{q} \right) + j_{BM,net} \cdot \left(\frac{\Delta E_{e/f}}{q} \right) + j_{rec} \cdot \frac{E_G'}{q}. \tag{20}$$

The recombination current density can be determined from Eqs. (17) and (20) only if $j_{EM,net}$ and $j_{BM,net}$ are known. The current paths in a standard PERC solar cell under open-circuit conditions including effects of lateral current transports are therefore analyzed in the following.

The distribution between the electrons/holes that travel exclusively in the emitter/base, respectively, and the ones that cross into the metallization on their way to the recombination site depends strongly on the emitter sheet resistance, the base resistivity, the contact resistance, and on the recombination rate of and distance to the recombination-active site. All these parameters influence the local gradient of the electrochemical potential.

In order to give an idea about the relative distributions, we performed device simulations employing Quokka3 [16]. We chose the PERC input parameters from Ref. [17] representing typical industrial PERC solar cells. Here, the rear side consists of line-shaped parallel contact openings. The simulation parameters most important for this work are listed in Table 2. In order to take also long-range effects into account, a whole quarter of a cell was simulated, see Fig. 3. At the center of the domain, a defect cluster of size 4 mm × 4 mm was placed. In order to investigate the influence of its recombination activity, the saturation current density J_0 caused by the defect cluster was varied between 50 fA/cm^2 and 3.5 pA/cm^2 covering an ample range of possible defect impacts. In addition, the generation rate was swept from 0.05 to 1 sun equivalent, a common intensity range for Suns-ILIT.

The current distributions for both majority carriers under V_{OC} conditions were analyzed. Since the defect cluster is the only feature with a significant recombination activity, it is clear that it dominates the lateral current distribution. In general, three different regions can be distinguished.

In the first region far away from the defect cluster, a small amount of the generated current is collected by the metallization – i.e. the nearest finger – and travels to the defect cluster through the fingers and busbars. The amount of these collected carriers is laterally constant, i.e. the distance to the defect cluster plays only a negligible role as long as the contact resistance and resistivity of the metallization are low compared to the emitter sheet resistance. The rest of the generated current recombines locally. The long-range transport therefore happens exclusively through the metallization.

In region 3, the defect cluster itself, all locally generated carriers recombine. In addition, carriers arrive through the metallization directly crossing the cluster and recombine.

In region 2, lying just outside the defect cluster, majority carriers travel to the recombination site through the silicon bulk/emitter. Our simulations show that the maximum extent of this region is only to the nearest neighboring finger that does not cross the defect cluster. In the direction along the fingers that cross the defect region, the extent is slightly larger, cf. Fig. 3.

The main result is hence that in this case, Eqn. (19) can be simplified to

$$j_{EM,net}, j_{BM,net} = j_{pn,net}$$

in places of electrical contact (besides the trivial $j_{EM,net}, j_{BM,net} = 0$ where there is none).

In principle, with this information, $j_{pn,net}$ and with it j_{rec} can be calculated. However, this would require to distinguish laterally exactly between fingers and the regions in between, which makes the analysis unpractical. Instead, we argue that (i) the relevant order of magnitude of the distances involved is half the finger pitch, because this is the maximum distance the majority carriers travel through emitter / base before entering (locally releasing Peltier heat in the regions far away from the recombination-active sites) or after leaving (Peltier cooling very close by recombination-active sites) the metallization; (ii) the images are thermally blurred with a thermal diffusion length – for a standard lock-in frequency of 30 Hz – of around 1 mm. Since this is more than half the finger pitch in many cases, this influence is not resolved. In addition, generally the pitch of the metallization is determined by the doping concentration, with wider pitches coming along with higher doping concentrations. As the Peltier coefficients decrease with increasing doping concentrations, as shown in the next section, their importance decreases with increasing pitch.

These statements are supported by our experimental observation that in general, we cannot attribute any distinct features to local Peltier heating and cooling even in high-resolution and emissivity-corrected V_{OC}-ILIT images of standard PERC solar cells (not shown here). Due to a smaller signal-to-noise ratio, higher lock-in frequencies with lower thermal diffusion lengths are highly uncommon.

Therefore, we propose that

$$j_{pn,net} = \frac{p_{in} - p}{V_{OC}} \tag{21}$$

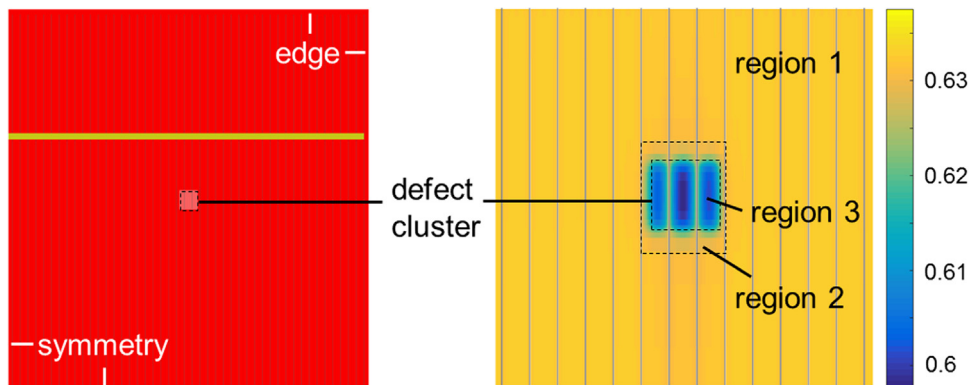is a good assumption for the case of both-side contacted solar cells. It

Fig. 3. Left: Sketch of the simulation domain; right: simulated emitter potential (in V) for the maximum J_0-value in the defect at 1 sun equivalent.

may have to be revised e.g. in the case of back contacted cells or other non-standard cell architectures.

2.2. The denominator: local V_{OC} and Peltier coefficients

For a precise determination of the local recombination current, a good knowledge of the denominator in Eqs. (16) and (21) is essential which may comprise the local open-circuit voltage and the positions of the majority carriers in their respective energy bands.

The open-circuit voltage may vary laterally depending on the illumination conditions [5]. Whereas the voltage variation is negligible at low injection (< ~1/10 sun equivalent), it can reach several 10 mV under an illumination equivalent to 1 sun. Therefore, it is advisable to obtain a set of implied V_{OC} measurements as e.g. used for Suns-PLI in addition to ILIT measurements. It has to be noted that the implied V_{OC} determined by PLI deviates from the terminal (pn junction) voltage measured by the Suns-V_{OC} technique when going to high injection levels [18,19]. However, up to ~ 1 sun equivalent, the difference is negligible.

For the Peltier heating component, the actual positions of the carriers within the energy bands and their contributions to the current have to be considered [15]. In fact, the physical quantities $\Delta E_{e/f}$ and $\Delta E_{f/h}$ can be identified with the majority carrier Peltier coefficients in the emitter and base, respectively (p-type base assumed) [15]. They strongly depend on the doping level.

For practical use, we fitted literature data of the Peltier coefficients taken from [20–22] to the power law

$$\frac{\Delta E_i}{q} = a + b \cdot \left(\frac{N_j}{N_0}\right)^c ,$$
(22)

where the indices i and j represent e/f and D for the n-type region of the pn junction and f/h and A for the p-type region, respectively. The parameters are listed in Table 1. For a typical p-type silicon solar cell with a base resistivity of 1 Ωcm ($N_A = 1.4 \times 10^{16}$ cm^{-3}) and a diffused emitter with phosphorus concentration of ~1 × 10^{20} cm^{-3} at the surface, Peltier voltages of 408 mV and 62 mV, respectively, are expected. In comparison, Peltier coefficients in the metallization are in the order of ~1 mV and thus negligible [15] (Fig. 4).

Fit parameters to Eq. (22) for the Peltier coefficients as reported in literature [21–23].

2.3. Local I-V

The calculation of the recombination current density images from non-contacted illuminated samples gives per se already useful information. In conjunction with the variation of the illumination intensity, it provides a simple but powerful means for solar cell characterization. The principle is the same as in Suns-V_{OC} measurements: The variation in illumination entails both a variation in the photo-generated (recombination) current and in (local) voltages. Via ILIT and PLI, we have position-dependent information of both and hence the local I-V-characteristic corresponding to the local Suns-V_{OC} curve can be evaluated.

In practice, however, the illumination-varied ILIT measurements impose some restrictions on the I-V analysis: At very low illumination intensities, the potential gradients driving the lateral currents become

Table 1
Parametrization of the Peltier Coefficient of p- and n-type Silicon at 300 K.

Parameter	P-TYPE SI	n-type Si
a	0.550 V	0.753 V
b	-5.708×10^{-4} V	-0.02332 V
c	0.14835	0.07362
N_0	1 cm^{-3}	

Table 2
Parameters used for the Quokka3 simulation of a standard PERC solar cell.

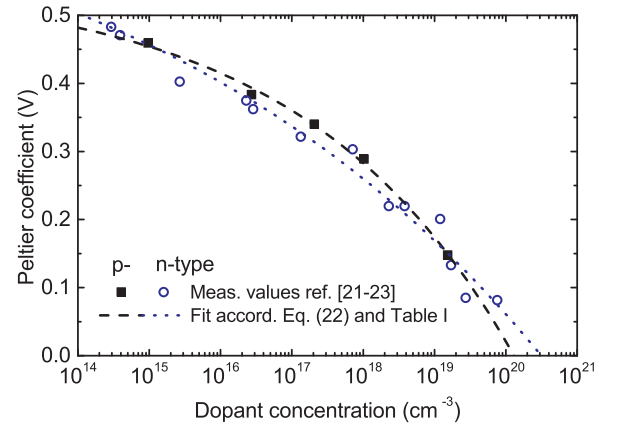| Parameter	VALUE
Base resistivity	2 Ωcm (p)
Emitter sheet resistance	160 Ω/sq (n)
Contact resistance (front/rear)	2×10^{-3} Ωcm^2
Finger width (front)	60 µm
Pitch (front)	1.7 mm
Contact opening width (rear)	120 µm
Pitch (rear)	850 µm

Fig. 4. Measured Peltier coefficients as a function of dopant concentration [20–22] and the parameterization proposed in the text.

very small. In addition, the measurement signal is very low. Therefore, lateral signal contrasts are almost imperceptible. Since in Suns-V_{OC} measurements, the low-intensity region is used to evaluate the shunt resistance R_p, the latter is difficult to assess quantitatively.

Besides this limitation, all other solar cell parameters that can be found globally via Suns-V_{OC} are also accessible by Suns-ILIT. An established way to do this is based on the iteration method introduced by Breitenstein [10] for the "local I-V" analysis. An example for this approach is presented in Section IV.

3. Experimental

The ILIT images for the following Suns-ILIT evaluations are taken using a camera sensitive in the mid-infrared wavelength range between $1.5 - 5$ µm with a stirling-cooled InSb-FPA of size 512×512 pixels. The sample is positioned on an actively temperature-controlled stage ($T = 25\,°C$) and is homogeneously illuminated via two LED arrays at opposing sides of the sample stage. The monochromatic illumination wavelength is 950 nm. The illumination intensity is calibrated via a reference solar cell. To achieve low illumination intensities below 0.1 sun equivalents, neutral-density filters are used. At last, the images are corrected for the influences of inhomogeneous emissivity [23].

The lateral implied V_{OC} distributions are calculated from calibrated PLI measurements taken at the same generation rates as the ILIT measurements [8]. The samples are illuminated using a 790 nm laser; we assume that the impact of the difference in the carrier distribution due to the different absorption depths is negligible. Again, the samples are kept at a constant temperature of 25 °C.

To demonstrate the Suns-ILIT method, a multicrystalline silicon PERC solar cell (p-type base) processed at Fraunhofer ISE PV-TEC was chosen, representing current standard technology [24]. In order to highlight the potential benefits of the camera-based measurement method, the solar cell was selected due to a slightly increased j_{02} value, as indicated by the global I-V characteristic, and a relatively high j_{01}
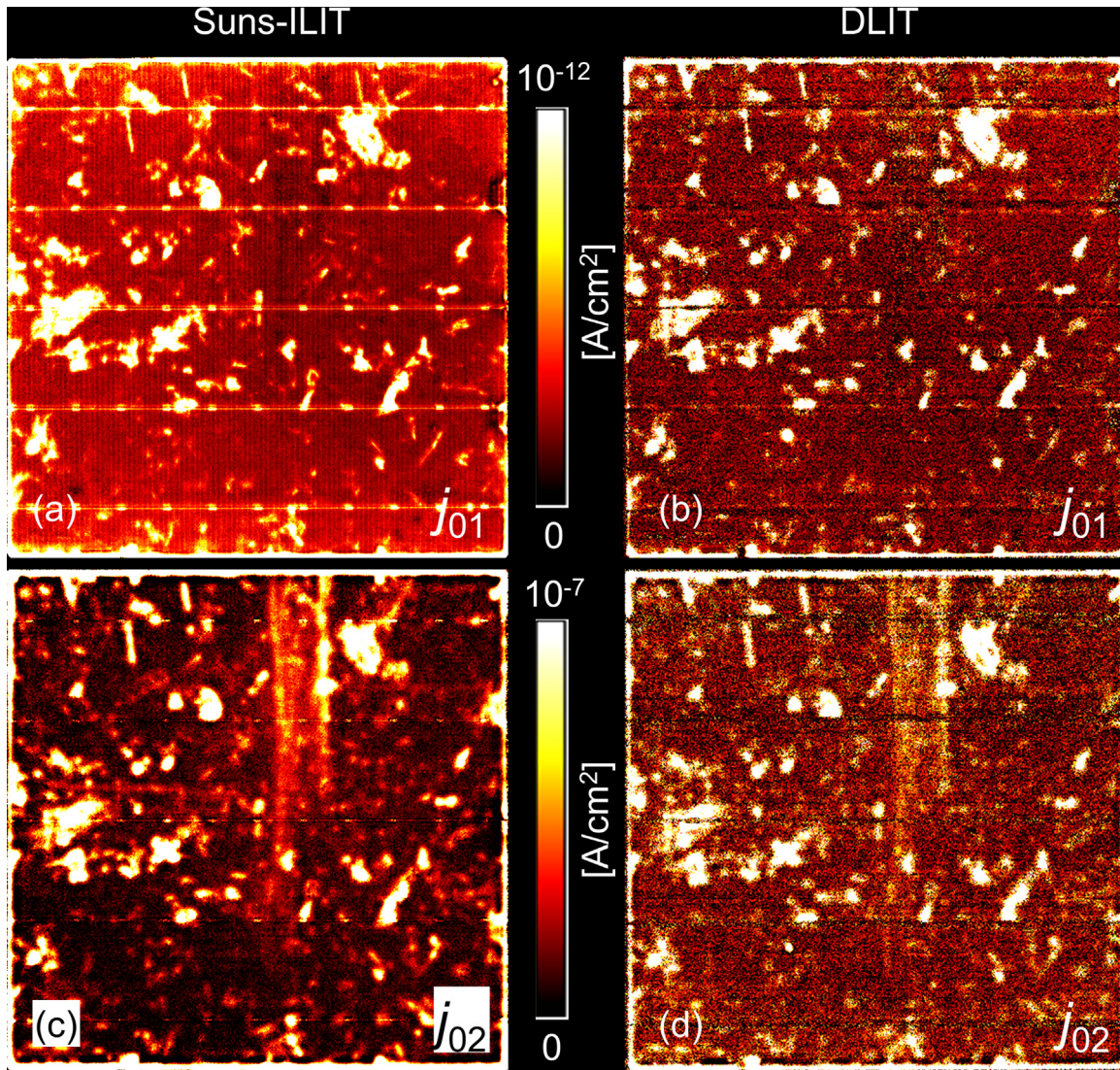
Fig. 5. j_{01} distribution employing Suns-ILIT (a) and DLIT (b), j_{02} distribution based on Suns-ILIT (c) and DLIT (d) using "local *I-V*"[10] with n_2 set to 2. The black background was chosen to be able to discern the high measurement signal at the cell edges.

Table 3
Comparison between Parameters J_{01} and J_{02} from different methods.

Method	J_{01} [fA/cm²]	j_{02} [nA/cm²]
Suns-V_{OC}	385	22.3
Suns-ILIT (av.)	344	24.3
Dark I-V	319	19.2
DLIT (av.)	254	28.8

value due to the multi-crystallinity. The following analysis is only meant to give a short example. A thorough investigation of the method, its possibilities as characterization tool for solar cell precursors and a detailed comparison to common global solar cell parameters obtained via dark and light *I-V* characteristics and Suns-V_{OC} measurements are topic of a future publication.

4. Exemplary results

Since single images of the distribution of recombination current densities are not very meaningful by themselves at this point, Fig. 5(a) and (c) show the j_{01}- and j_{02}-distribution, respectively, of the sample cell using Suns-ILIT measurements for the "local *I-V*" analysis following

Ref. [10] with n_2 set to 2. In this way, the quality of the recombination current density quantification can be assessed.

For comparison, Fig. 5(b) and (d) display the same physical quantities as above, but this time acquired via conventional DLIT measurements. To increase accuracy, a measurement of the series resistance distribution using the "coupled determination of the dark saturation current and series resistance" method (C-DCR) [7] was added to the analysis [10,11].

In addition, the arithmetically averaged j_{01}- and j_{02}-values obtained using Suns-ILIT and DLIT are compared to the values measured by means of Suns-V_{OC} and dark I-V in Table 3.

It can be seen that, in general, both methods for measuring the local *I-V* characteristics give similar results, giving a first indication for the accuracy of the Suns-ILIT measurements. Compared to the global values, Suns-ILIT matches relatively well to the Suns-V_{OC} data, whereas the DLIT-based analysis overestimates j_{02} to some extent in this case. For a detailed evaluation and comparison to other methods, the reader is referred to a future contribution.

Having a closer look, j_{01} is dominated by recombination in defect clusters, whereas very high j_{02} values are measured at the cell edges. Both Suns-ILIT and DLIT successfully discriminate an additional significant feature which is attributed to j_{02} and cannot be seen in j_{01}: two parallel lines at the top extending towards the cell center, probably a

result of a non-optimal wet chemical process. In addition, Suns-ILIT is able to resolve the recombination currents at the metallization whereas both the front busbars and the rear contacts are shadowed by the contacting frame in the case of DLIT, illustrating one of the advantages of Suns-ILIT.

It is generally accepted that j_{01} signifies the saturation current density due to recombination in the bulk and at the surfaces, whereas j_{02} describes recombination in the depletion region. High values of j_{02} at defect clusters (cf. Fig. 5(c) and (d)) are therefore unexpected. Nevertheless, similar local *I-V* results have been shown previously [11,25] and several hypotheses were discussed, e.g. insufficient separation of both diodes due to variable ideality factors. A detailed analysis is currently under way.

The most prominent difference between both methods lies in the distribution of the background values. In Suns-ILIT in particular, the homogeneously distributed background j_{01} is obvious. The difference between the methods may be explained as a direct result of the fundamentally different excitation strategies (cf. Ref [26]): In DLIT, an external bias is applied to the busbars, driving a dark current which follows the path of least resistance. The excitation is therefore relatively inhomogeneous; for example, in good cell areas, only very small currents flow. By contrast, in Suns-ILIT, carriers are generated homogeneously – as under real operating conditions – and recombine following the distribution of the electrochemical potential. Due to this homogeneous excitation, significant currents flow also in the good solar cell areas, increasing the local background signal.

Please note that in principle, the noise seen especially in Fig. 5(b) – (d) is mostly a matter of detector sensitivity and measurement time and is not an intrinsic, fundamental property of the measurement strategy.

5. Conclusion

Suns-ILIT is a highly useful technique as it overcomes several drawbacks of conventional methods to assess the global or local *I-V* characteristics:

- No electrical contacts are needed. Hence, besides solar cells, also un-metallized solar cell precursors can be investigated. By employing an emissivity correction, contributions of the metallization to the recombination currents can be quantitatively assessed.
- Deriving the local current density from images of the local power dissipation and the local (implied) voltage under V_{OC} conditions, i.e. combining ILIT with PLI, the accuracy of local *I-V* characteristics can be greatly enhanced compared to Suns-V_{OC} or methods e.g. based exclusively on PLI, and is still an entirely contactless approach.
- The possibility to use different wavelengths opens up interesting new fields of application. One possible example is the use in tandem devices.

Acknowledgment

References

[1] R.A. Sinton, A. Cuevas, A quasi-steady-state open-circuit voltage method for solar cell characterization, in: Proceedings of the 16th European Photovoltaic Solar Energy Conference, Glasgow, Scotland, 2000, pp. 1152–1155.

[2] C.-t. Sah, R. Noyce, W. Shockley, Carrier generation and recombination in P-N junctions and P-N junction characteristics, Proc. IRE 45 (9) (1957) 1228–1243.

[3] T. Trupke, R.A. Bardos, M.D. Abbott, J.E. Cotter, Suns-photoluminescence: contactless determination of current-voltage characteristics of silicon wafers, Appl. Phys. Lett. 87 (9) (2005) 93503.

[4] Z. Hameiri, P. Chaturvedi, Spatially resolved electrical parameters of silicon wafers and solar cells by contactless photoluminescence imaging, Appl. Phys. Lett. 102 (7) (2013) 73502.

[5] B. Michl, D. Impera, M. Bivour, W. Warta, M.C. Schubert, Suns-PLI as a powerful tool for spatially resolved fill factor analysis of solar cells, Prog. Photo. Res. Appl. 22 (5) (2014) 581–586.

[6] D. Hinken, K. Ramspeck, K. Bothe, B. Fischer, R. Brendel, Series resistance imaging of solar cells by voltage dependent electroluminescence, Appl. Phys. Lett. 91 (18) (2007) 182104.

[7] M. Glatthaar, et al., Spatially resolved determination of dark saturation current and series resistance of silicon solar cells, Phys. Status Solidi RRL 4 (1–2) (2010) 13–15.

[8] M. Glatthaar, et al., Evaluating luminescence based voltage images of silicon solar cells, J. Appl. Phys. 108 (1) (2010) 14501.

[9] C. Shen, et al., Spatially resolved photoluminescence imaging of essential silicon solar cell parameters and comparison with CELLO measurements, Sol. Energy Mater. Sol. Cells 109 (2013) 77–81.

[10] O. Breitenstein, Nondestructive local analysis of current–voltage characteristics of solar cells by lock-in thermography, Sol. Energy Mater. Sol. Cells 95 (10) (2011) 2933–2936.

[11] O. Breitenstein, Local efficiency analysis of solar cells based on lock-in thermography, Sol. Energy Mater. Sol. Cells 107 (2012) 381–389.

[12] J. Isenberg, W. Warta, Realistic evaluation of power losses in solar cells by using thermographic methods, J. Appl. Phys. 95 (9) (2004) 5200–5209.

[13] O. Breitenstein, W. Warta, M. Langenkamp (Eds.), Lock-in Thermography: Basics and Use for Evaluating Electronic Devices and Materials, 2nd ed, Springer, Heidelberg, New York, 2010.

[14] O. Breitenstein, J.P. Rakotoniaina, Electrothermal simulation of a defect in a solar cell, J. Appl. Phys. 97 (7) (2005) 74905.

[15] H. Straube, Quantitatives Verständnis von Lock-in-Thermographie an Dünnschicht-Solarmodulen, Ph.D. Thesis, Naturwissenschaftliche Fakultät II, Martin-Luther-Universität Halle-Wittenberg, Halle (Saale), 2011.

[16] A. Fell, J. Schön, M.C. Schubert, S.W. Glunz, The concept of skins for silicon solar cell modeling, Sol. Energy Mater. Sol. Cells 173 (2017) 128–133.

[17] A. Fell, et al., Input parameters for the simulation of silicon solar cells in 2014, IEEE J. Photovolt. 5 (4) (2015) 1250–1263.

[18] M.K. Juhl, T. Trupke, The impact of voltage independent carriers on implied voltage measurements on silicon devices, J. Appl. Phys. 120 (16) (2016) 165702.

[19] R. Dumbrell, M.K. Juhl, T. Trupke, Z. Hameiri, Comparison of terminal and implied open-circuit voltage measurements, IEEE J. Photovolt. 7 (5) (2017) 1376–1383.

[20] T.H. Geballe, G.W. Hull, Seebeck effect in silicon, Phys. Rev. 98 (4) (1955) 940–947.

[21] M.E. Brinson, W. Dunstant, Thermal conductivity and thermoelectric power of heavily doped n-type silicon, J. Phys. C Solid State Phys. 3 (3) (1970) 483 ⟨http://stacks.iop.org/0022-3719/3/i=3/a=001⟩.

[22] L. Weber, E. Gmelin, Transport properties of silicon, Appl. Phys. A 53 (2) (1991) 136–140, https://doi.org/10.1007/BF00323873.

[23] M. Kasemann, et al., Emissivity-corrected power loss calibration for lock-in thermography measurements on silicon solar cells, J. Appl. Phys. 103 (11) (2008) 113503.

[24] J.M. Greulich et al. Increasing the efficiency of industrial multicrystalline silicon PERC solar cells from currently 19 to 20%, in: Proceedings of the 33rd EU PVSEC, Amsterdam, The Netherlands, 2017.

[25] O. Breitenstein, F. Frühauf, J. Bauer, Advanced local characterization of silicon solar cells, Phys. Status Solidi A 214 (12) (2017) 1700611.

[26] A.G. Aberle, S.R. Wenham, M.A. Green, A new method for accurate measurements of the lumped series resistance of solar cells, in: Proceedings of the 23rd IEEE Photovoltaic Specialists Conference Louisville, Louisville, 1993, pp. 133–139.